Cellulose (2019) 26:4005–4019
https://doi.org/10.1007/s10570-019-02328-w

ORIGINAL RESEARCH

Enhanced heavy metal adsorption ability of lignocellulosic hydrogel adsorbents by the structural support effect of lignin

Xiaoping Shen · Yanjun Xie · Qingwen Wang · Xin Yi · Julia L. Shamshina · Robin D. Rogers

Received: 29 November 2018 / Accepted: 20 February 2019 / Published online: 6 March 2019

Abstract Cellulose beads possess some adsorption capacities for heavy metal ions, but the effect of lignin remaining in the beads on the adsorption behavior is not clear yet. In this study, lignocellulosic and cellulosic hydrogel beads were prepared by ionic liquid (IL) dissolution and reconstitution in water and further functionalization through magnetization and carboxymethylation. Compared to pure cellulosic beads made from Kraft pulp and microcrystalline cellulose, the presence of lignin in the lignocellulosic beads from IL-extracted cellulose-rich material (CRM) helped support the porous structure, leading to a higher hydroxyl number and porosity, and thus higher efficacy in magnetization and carboxymethylation. CRM beads, therefore, exhibited greater Cu^{2+} and Pb^{2+} uptake than the cellulosic beads both before and after modification. However, excessive lignin in the beads prepared directly from poplar wood powder caused negative effects on the adsorption capacity due to agglomeration and occlusion of the adsorptive sites.

Electronic supplementary material The online version of this article (https://doi.org/10.1007/s10570-019-02328-w) contains supplementary material, which is available to authorized users.

X. Shen · Y. Xie (✉) · X. Yi
Key Laboratory of Bio-based Material Science and Technology (Ministry of Education), College of Material Science and Engineering, Northeast Forestry University, 26 Hexing Road, Harbin 150040, China
e-mail: yxie@nefu.edu.cn

X. Shen
School of Engineering, Zhejiang A & F University, Lin'an 311300, China

Q. Wang (✉)
College of Materials and Energy, South China Agricultural University, 483 Wushan Road, Guangzhou 510642, China
e-mail: qwwang@scau.edu.cn

J. L. Shamshina
Mari Signum Mid-Atlantic, LLC, 3204 Tower Oaks Boulevard, Rockville, MD 20852, USA

R. D. Rogers
525 Solutions, Inc., P.O. Box 2206, Tuscaloosa, AL 35403, USA

Graphical abstract

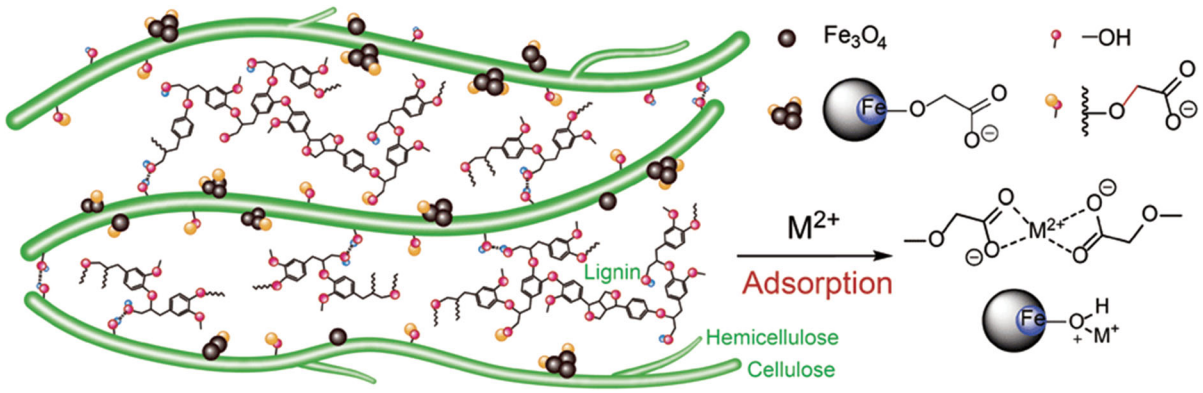

Keywords Lignocellulosic hydrogel beads · Structural support · Hydroxyl number · Heavy metal adsorption

Introduction

Adsorption is an efficient strategy for removing heavy metals from polluted water bodies (Liu et al. 2015; Thakur et al. 2017). Lignocellulosic biomasses, e.g., wood sawdust, can technically be used to adsorb heavy metals, but the adsorption capacity is very low—about 0.04 and 0.02 mmol g^{-1} for Cu^{2+} and Pb^{2+} adsorption, respectively (Gan et al. 2016; Sciban et al. 2006). This is attributed to (a) the low specific surface area of the material (Sciban et al. 2006), (b) the insufficient exposure of adsorptive sites (hydroxyl groups, –OH) in fibers which feature an integral cell wall structure (Barnett and Bonham, 2004), and (c) the relatively weak affinity or complexation between the lone pair electrons of oxygen atoms in the –OH groups and the metal ions (Shen et al. 2016a), when compared to, for instance, carboxyl or carboxyalkyl (Chen et al. 2009; Yu et al. 2013), phosphorus (Jeon and Kim, 2009), nitrogen (Donia et al. 2012), or sulfur-containing groups (Wu et al. 2012).

To improve the adsorption ability of lignocellulosic materials, the cell wall layer structure is usually disintegrated to expose cellulosic nanofibrils (CNFs) and therefore produce greater specific surface area and more abundant accessible hydroxyl groups (Sehaqui et al. 2014). During this process, lignin, a biopolymer present in lignocelluloses and generally composed of a carbon–oxygen framework with various functional groups (methoxyl, phenol, ether, etc.) is commonly removed during adsorbent production since it has a lower number of surface-accessible acidic hydroxyl groups than cellulose does, per absorbent mass, and therefore is considered as a "filler". Such removal of lignin further increases the number of accessible hydroxyl groups per unit area in the CNFs. However, both cell wall disintegration and lignin removal require intensive mechanical grinding coupled with chemical purification and consequently, the preparation process of CNFs is highly energy-consumptive (Chen et al. 2013). Additionally, the disposal of lignin and chemicals used for treatment, e.g., the black liquor produced from the pulp industry (Pokhrel and Viraraghavan 2004), is also a big challenge.

There is an alternative for the exposure of hydroxyl groups by reconstructuring the biopolymers into either hydrogels (Shen et al. 2016a; Thakur et al. 2018) or areogels (Kim et al. 2017), in which the re-crystallization of the cellulose trains can be restrained or diminished. Expectedly, hydrogels prepared from lignin by chemically cross-linking with common cross-linkers such as formaldehyde, glutaraldehyde, α-epichlorohydrin, or diepoxy compounds generally exhibit low water content and low adsorption capacity attributed to the lower number of –OH groups, unless another active component is introduced (Thakura and Thakur 2015).

Concluded from above, hydrogels made from partially or entirely delignified lignocelluloses are supposed to possess maximum adsorption capacity compared with the pristine lignocellulosic biomasses. Since 2009, the Rogers group has reported that the

dissolution and regeneration of wood in the ionic liquid (IL) 1-ethyl-3-methylimidazolium acetate ([C_2mim][OAc]) produced free lignin and cellulose-rich materials (CRMs). The CRMs contained much lower lignin contents compared to the original wood (Cheng et al. 2014; Li et al. 2011a; Sun et al. 2009, 2011; Wang et al. 2012). In later work, they also showed that among all CRM pulps produced using various IL-dissolution methods, the CRM prepared by the dissolution of wood in [C_2mim][OAc] at a higher temperature (175 °C) for a shorter time (30 min) and regeneration in acetone/water as an anti-solvent had the highest molecular weight (MW) and the best hydrogel forming ability (Shen et al. 2016b).

However, on the other hand, considering that lignin has a stiff 3D polymeric network and thereby may help support hydrogel structure, lignin-containing pulps (e.g., CRMs) may provide opportunities for not only hydrogel production at higher yields but also improvements of the porosity, and thus adsorption properties of the resulting hydrogel adsorbent compared to the hydrogels based on fully-delignified cellulose pulps. In this study, we initially investigated the effect of lignin on the microstructure of the reconstituted lignocellulose by analyzing the regenerated aqueous suspensions from poplar wood powder (POP), CRM, Kraft pulp (KP), and microcrystalline cellulose (MCC) solutions in [C_2mim][OAc] via transmission electron microscopy (TEM). Subsequently, lignocellulosic hydrogel beads were prepared, by dissolving the POP or CRM pulp in [C_2mim][OAc], and reconstituted into a bead architecture using water as a coagulation solvent. These lignocellulosic beads as prepared were compared to hydrogel beads prepared from pure cellulose (MCC and KP) in terms of the properties including microstructure, number of hydroxyl groups, density, and porosity.

The original beads prepared were then functionalized by carboxymethylation, magnetization, or combined treatment with magnetization/carboxymethylation, to examine the effect of the presence of lignin on the functionalization efficacy of the lignocellulosic beads. Finally, the adsorption ability of the lignocellulosic and pure cellulosic hydrogel beads (both the original and the functionalized) towards Cu^{2+} and Pb^{2+} ions was studied and compared to verify the potential superiority of the lignocellulosic hydrogel beads over the pure cellulosic ones as bio-adsorbents.

Materials and methods

Chemicals and cellulosic materials

Ionic liquid 1-ethyl-3-methylimidazolium acetate ([C_2mim][OAc], 99%, 1900 ppm water content measured with a Metrohm 831 Karl Fischer Titrator, Beijing, China), was purchased from Chengjie Chemical Ltd., Shanghai, China. Other chemicals including pyridine, sodium hydroxide (NaOH), ferrous chloride hydrate ($FeCl_2{\cdot}4H_2O$), ferric chloride hydrate ($FeCl_3{\cdot}6H_2O$), absolute ethanol (EtOH), sodium monochloroacetate ($NaClCH_2COO$), cupric nitrate hydrate ($Cu(NO_3)_2{\cdot}3H_2O$), lead nitrate ($Pb(NO_3)_2$), and nitric acid (HNO_3; 65 wt%) were of analytical grade and used as received from Sigma Aldrich (Shanghai, China). Deionized (DI) water with specific resistivity of 7.8 MΩ cm at 25 °C was purchased from Rightleder Environmental Investment Group Inc., Harbin, China. Ultrapure water with specific resistivity of 18.2 MΩ cm at 25 °C was obtained from the Milli-Q Century System (Millipore, Billerica, MA, USA).

Four different polymers (two lignocellulose and two pure cellulose) were used for preparing hydrogels: (1) mechanically ground poplar wood powder (POP), of particle sizes ranging from 80 to 100 mesh, was supplied by Yongxu Co., Ltd., Harbin, China; (2) cellulose-rich material (CRM), which was prepared by dissolving 0.5 g poplar wood powder in 10 g [C_2mim][OAc] at 175 °C for 30 min followed by regeneration in 50% v/v acetone/H_2O (Li et al. 2011a; Shen et al. 2016b); (3) bleached softwood Kraft pulp (KP),which was provided by Ilim Group (St. Petersburg, Russia) and had a whiteness value of 88–90%; and (4) microcrystalline cellulose (MCC), which was obtained from Sigma Aldrich (Shanghai, China).

Transmission electron microscopy (TEM) of lignocellulose suspensions

The 1% lignocellulose- or cellulose-IL solution was coagulated in ultrapure water, washed, and ultrasonically treated to obtain 0.05% aqueous suspensions. The suspensions were respectively dropped onto conventional carbon-coated copper grids, and were vacuum dried at 25 °C for 1 h. TEM observation of the samples was conducted by using a JEOL JEM-2100

transmission electron microscope (Tokyo, Japan) at 200 kV.

Preparation of hydrogel beads from lignocellulose-IL solution

Note % load = mass of solute (g)/mass of solvent (g). POP (0.7 g) was dissolved in 20 g [C_2mim][OAc], in a 100 mL beaker at 175 °C in an oil bath under magnetic stirring for 30 min to obtain a 3.5% solution; CRM (0.4 g), KP (0.4 g), or MCC (1.0 g) was dissolved in 20 g of [C_2mim][OAc] at 100 °C for 1 h to obtain solutions of 2% CRM, 2% KP, or 5% MCC, respectively. The polymer concentrations were selected to guarantee both the fluidity of the solution and the strength of the resulting hydrogel beads.

The hot lignocellulose- or cellulose-IL solutions were quickly transferred from the beaker into a 5 mL plastic syringe and injected dropwise (without a needle) into a 500 mL Erlenmeyer flask containing 300 mL DI water (at room temperature, 21 °C), where the hot drops were fully cooled down to form hydrogel beads that won't stick together. (Please note that during the dropping process, the remaining solution in the beaker was stored in the oven at 80 °C. Water in the flask was frequently refreshed every two or three syringes to keep it cool.) The hydrogel beads in the Erlenmeyer flask were taken out and thoroughly washed repeatedly with DI water to completely remove [C_2mim][OAc] IL. The resultant original hydrogel beads were denoted as $POP_{3.5}$, CRM_2, KP_2, and MCC_5, respectively.

Yields of the beads were determined to be 74 (3)% for $POP_{3.5}$ (the moderate yield explained by the highest solution viscosity, and therefore the greatest difficulty during transfer into the syringe), 86 (2)% for CRM_2, 89 (3)% for KP_2, and 80 (2)% for MCC_5 (some MCC drops failed to form beads), respectively.

Functionalization of hydrogel beads

The original hydrogel beads were separated into four groups: one quarter was used for carboxymethylation treatment through a modified procedure previously reported (Qi et al. 2009), one quarter for magnetization through a slightly modified technique reported previously (Luo et al. 2009; Tang et al. 2014), one quarter for magnetization followed by carboxymethylation (details described in Electronic supplementary material), and the last quarter was used as untreated controls. The resultant carboxymethylated, magnetized, and dually modified beads were abbreviated as C (e.g., $CPOP_{3.5}$), M (e.g., $MPOP_{3.5}$), and MC-($MCPOP_{3.5}$) beads, respectively. Characterization methods including viscosity determination of the lignocellulose-IL solutions, Fourier transform-infrared spectroscopy (FT-IR), powder X-ray diffraction (PXRD), scanning electron microscopy (SEM), hydroxyl number determination, lignin analysis, density and porosity determination, substitution degree determination, and magnetic property test of the hydrogel beads, are described in Electronic supplementary material.

Heavy metal ion adsorption test

Erlenmeyer flasks (100 mL) each containing 25 mL of 0.1 mM $Cu(NO_3)_2{\cdot}3H_2O$ or $Pb(NO_3)_2$ solution (hereafter abbreviated as Cu^{2+} or Pb^{2+} solution) were kept in a SHA-C thermostatic incubator shaker (Ruihua Co., Ltd., Jintan, China) at 25 °C. The pH values of Cu^{2+} or Pb^{2+} solutions were adjusted to 4.0, 4.5, 5.0, 5.3, or 6.0 by adding 0.1 M HNO_3 or 0.1 M NaOH. Wet beads (0.04 g dry mass per 100 mL solution) were added to each conical flask shaken mechanically at 100 rpm for 24 h. The beads were then removed and the concentration of metal ions in the resulting solutions were determined using an atomic absorption spectrophotometer (AAS; Purkinje General TAS-990, Beijing, China) according to the calibration curves determined for the Cu^{2+} or Pb^{2+} ions (Fig. S1).

Adsorption isotherms and adsorption kinetics

The equilibrium sorption isotherms (at 25 °C) were obtained by recording the equilibrium ion concentrations of the solutions and the adsorption capacitors of the beads after immersing different amount of the wet beads (ca. 0.004–0.090 g dry mass per 100 mL solution) in 0.1 mM Cu^{2+} and Pb^{2+} solutions for 24 h at pH 6 for Cu^{2+} and pH 5.3 for Pb^2, respectively. The equilibrium sorption isotherms were then described via Langmuir, Freundlich and Sips models (Chatterjee et al. 2010; Ngah and Fatinathan 2008), which are presented using the equations below:

$$q_e = \frac{q_m K_L C_e}{1 + K_L C_e}$$

$$q_e = K_F C_e^{1/n}$$

$$q_e = \frac{q_{\max}(K_S C_e)\beta_S}{1 + (K_S C_e)^{\beta_S}}$$

where q_e (mmol g^{-1}) is the adsorption capacity of the sample at equilibrium, C_e (mM) the concentration of metal ions in solution at equilibrium, q_m (mmol g^{-1}), K_L (l $mmol^{-1}$), K_F, 1/n, q_{max} (mmol g^{-1}), K_S (l $mmol^{-1}$) and β_S the corresponding equation constants.

The kinetic adsorption experiments were also measured by immersing the wet beads (0.04 g dry mass per 100 mL solution) in a series of 0.1 mM Cu^{2+} and Pb^{2+} solutions at pH 6 for Cu^{2+} and pH 5.3 for Pb^{2+}, respectively, and shaking for different time intervals. Several adsorption kinetic models such as pseudo-first order, pseudo-second order and intra-particle diffusion kinetic models (Ngah and Fatinathan 2008, 2010) were used to understand the adsorption kinetics and the rate limiting step during adsorption process. The kinetic models are given as:

$$ln(q_e - q_t) = lnq_e - k_1 t$$

$$\frac{t}{q_t} = \frac{1}{k_2 q_e^2} + \frac{t}{q_e}$$

$$q_t = k_{\text{int}} t^{1/2} + C$$

where q_t (mmol g^{-1}) is the ion amount adsorbed onto the beads at time t, k_1 (h^{-1}), k_2 (g $mmol^{-1}$ h^{-1}), k_{int} (mmol g^{-1} $h^{1/2}$) are the rate constants of kinetic models, and C is the intercept which is associated to the boundary layer thickness.

Results and discussion

Regenerated lignocellulosic suspensions before attempting the fabrication of hydrogel beads

For the purpose of comparing the lignin-containing lignocellulosic hydrogel beads with the pure cellulosic ones in their properties and adsorption ability, we initially needed to identify what role, if any, lignin plays in the microstructure of the regenerated lignocellulose fibrils. Therefore, before attempting the fabrication of hydrogel beads, we coagulated poplar wood powder (POP), cellulose-rich material (CRM), Kraft pulp (KP), and microcrystalline cellulose (MCC) IL solutions in ultrapure water as the anti-solvent to produce 0.05 wt% aqueous suspensions. These suspensions were dropped on carbon-coated copper grids, ultrasonicated and vacuum-dried. The remnants after drying of the suspension was analyzed using TEM.

Interestingly, the remnants from lignin-free KP and MCC suspensions exhibited a higher degree of fibril entanglement where individual fibrils in pure suspensions could not be seen (Fig. 1a, b). However, entanglement phenomenon in the remnant from lignin-contained CRM was considerably less (Fig. 1c). The remnant from POP suspension, which has a higher lignin content than CRM as observed from the aromatic skeletal vibrations of lignin at 1589/1506 cm^{-1} in FT-IR (Labbe et al. 2005) in Fig. S2, displayed a great number of lignin globule aggregates (black spots in Fig. 1d).

The higher polymer entanglement in pure regenerated cellulose (Scheme 1a) can be attributed to the strong interaction between the pure cellulosic fibrils via hydrogen bonds. It can be inferred that a relatively low content of residual lignin in the CRM, as a three dimensional stiff macromolecular network, may restrict the approach of cellulosic fibrils thereby reducing formation of hydrogen bonds between the hydroxyl groups of the polysaccharide polymers (Scheme 1b). As the result, the entanglement of the polymer chains is inhibited, and the hydroxyl groups remain freely accessible. However, excessively high amount of hydrophobic lignin (e.g., POP) may create large "lignin globules" in POP suspensions (Scheme 1c), thereby covering the polysaccharides, and inhibiting the accessibility of the hydroxyl groups. In addition, the branched molecular structure of residual hemicellulose in CRM or POP may also impede the cellulosic polymers from forming denser fibril aggregates (Duchesne et al. 2001).

Preparation and characterization of cellulosic beads prior to derivatization

Having clarified the effect of lignin on the microstructure of the regenerated lignocellulose fibrils, we then

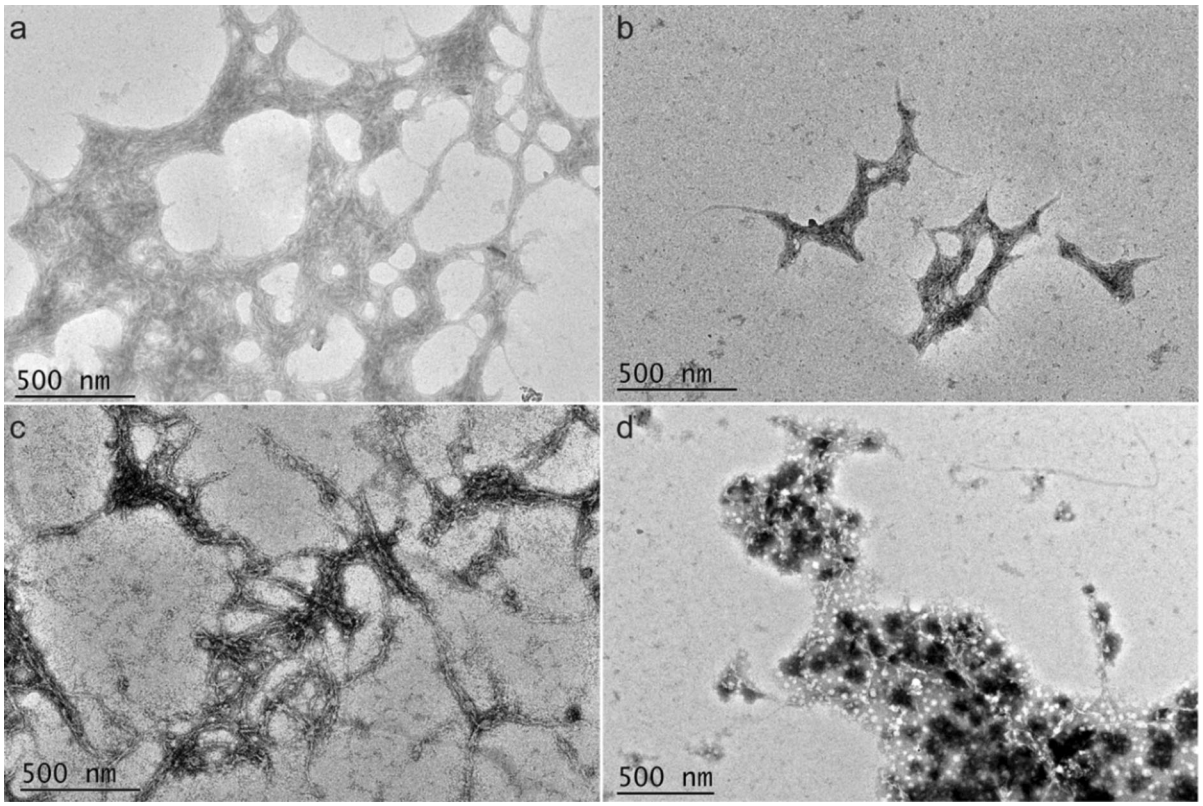

Fig. 1 TEM micrographs of the dry remnants obtained from the cellulose (**a** Kraft pulp—KP, **b** microcrystalline cellulose—MCC) or lignocellulose (**c** CRM, **d** poplar wood powder—POP) aqueous suspensions (0.05 wt%) after regenerating IL solutions with ultrapure water, ultrasonically treating, and vacuum drying on carbon-coated copper grids

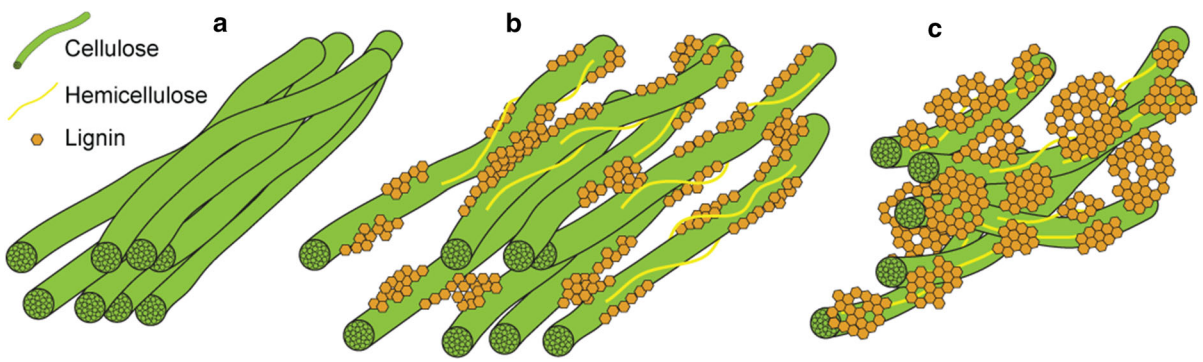

Scheme 1 Diagrammatic illustrations of the interaction between the macromolecules in 0.05 wt% aqueous suspensions of the regenerated cellulose (**a** KP or MCC) or lignocellulose (**b**: CRM, **c** poplar wood powder—POP)

proceeded to the preparation and comparison of the hydrogel beads. The cellulosic and lignocellulosic raw powder used could be reconstituted to form hydrogel beads from their [C_2mim][OAc] solutions by dropping the solutions into water anti-solvent. The appropriate concentrations of the solutions were found to be 3.5% for POP, 2% for KP, 2% for CRM, and 5% for MCC. At these concentrations the corresponding lignocellulose- and cellulose-IL solutions showed a proper viscosity or fluidity for the following beads preparation (Fig. S3). The pure cellulosic beads (KP_2 and MCC_5) appeared white, while lignocellulosic beads

($POP_{3.5}$ and CRM_2) looked yellow (Fig. S4, insets) due to the presence of lignin (Table 1). The CRM_2, KP_2, and MCC_5 original beads were round and exhibited a Gaussian-like distribution in diameter, with mean diameters of approximate 3.78, 2.52, and 3.60 mm, respectively (Fig. S4). This suggests that the presence of residual lignin and the higher substance mass are favorable factors in achieving larger diameter values. The 3.5% POP solution was extremely hard to form droplets due to the highest viscosity, resulting in ellipsoid-like $POP_{3.5}$ beads with an average minor axis as low as 2.24 mm (Fig. S4).

The freeze-dried beads exhibited a porous, low crystalline (Fig. S5), three-dimensional architecture with thin lamellar walls (Fig. 2). The macro-pores were interconnected, allowing access of the adsorbate (e.g., metal ion solution) to the adsorptive sites. The lamellar walls of the lignocellulosic beads ($POP_{3.5}$ and CRM_2) were in ordered alignment and the interior had a wood cell-like porous structure (Fig. 2a, b). Compared to the lignocellulosic beads, the pore structure of the pure cellulosic beads (KP_2 and MCC_5) appeared less ordered and some even collapsed (Fig. 2c, d), which may be due to formation of hydrogen bonds between polysaccharide polymers. At higher magnifications (5000–10,000 ×), micro-pores can be observed on the rough walls of the lignocellulosic beads, while the cellulosic beads exhibited smooth and dense walls. The ordered macro-porous structure and presence of micro-pores in the walls of lignocellulosic beads can be attributed to the stiff macromolecular network of lignin in the beads that can support the micro- and/or macro-porous structure and restrict the formation of hydrogen bonds. Such increase in the amount of the nano-scale pores due to the presence of lignin was also found in literature, which was observed by the specific surface area for nanofibrillated cellulose suspensions (Ferrer et al. 2012) and calorimetric thermoporometry for delignified biomass (Driemeier et al. 2016).

The CRM_2 beads had a lignin content of 12.0 (4)% that was comparable to the raw CRM powder (12.2 (3)%) (Shen et al. 2016b), which were approximately half that of the original wood (22.3 (6)%; Table 1). The lower lignin content was mainly attributed to the leaching of lignin from the IL-dissolved wood powder to the acetone/water solution during preparation of CRM powder (175 °C). The second dissolution from CRM powder to CRM_2 hydrogel beads did not cause further reduction in lignin content, because the IL dissolution was performed under more mild condition (100 °C) and the dissolved hydrophobic lignin would only be slightly leached into water. Compared to the CRM_2 beads, $POP_{3.5}$ had a higher lignin content (18.4 (4)%), which can be explained by the fact that $POP_{3.5}$ beads only underwent one IL dissolution process and were reconstituted in water.

Lignin in the lignocellulosic beads is approximately the "native lignin" after dissolution in the non-derivative IL solvent and reconstitution in water anti-solvent, which has a high degree of polymerization and thus a low phenolic hydroxyl number. The

Table 1 Lignin content, hydroxyl number, density, porosity, and water content of the hydrogel beads

Beads	Lignin content (%)	–OH number[a] (mmol KOH g^{-1})	Density[b] ($\times 10^{-2}$ g cm^{-3})	Porosity[c] (%)	Water content[d] (wt%)
Wood powder	22.3 ± 0.6	12.9 ± 0.4	ND	ND[e]	ND[e]
$POP_{3.5}$	18.4 ± 0.4	25.8 ± 0.6	9.9 ± 0.6	94.2 ± 0.5	95.6 ± 0.4
CRM_2	12.0 ± 0.4	28.7 ± 0.4	4.2 ± 0.3	97.0 ± 0.3	97.0 ± 0.4
KP_2	ND	23.2 ± 0.3	6.7 ± 0.2	95.4 ± 0.3	96.8 ± 0.2
MCC_5	ND	19.4 ± 0.2	11.3 ± 0.2	93.2 ± 0.2	93.6 ± 1.1

ND not detected

[a]Hydroxyl number of the wet beads

[b]Density of the freeze-dried beads

[c]Porosity of the wet beads

[d]Estimated based on the masses of the beads before and after oven drying

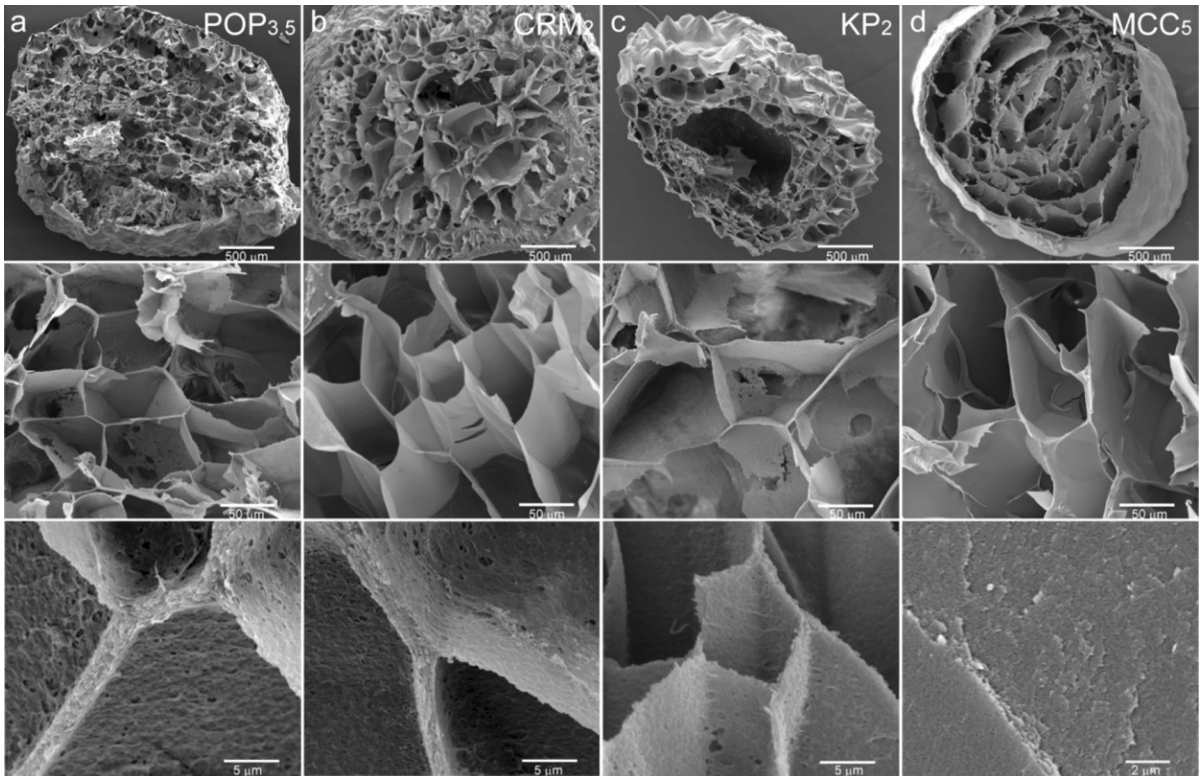

Fig. 2 SEM micrographs of $POP_{3.5}$ (Column **a**), CRM_2 (Column **b**), KP_2 (Column **c**), and MCC_5 beads (Column **d**) at different magnifications (the scale bars are 500, 50, 5 or 2 µm, respectively)

hydrogel beads prepared in this study had more accessible –OH groups than the pristine wood powder (Table 1), which was attributed to the exposure of the hydroxyl groups by disintegration of the cell wall structure and delignification of the resulting cell wall compositions.

Among all beads, the CRM_2 beads possessed the largest number of –OH groups (28.7 mmol KOH g^{-1}), followed by $POP_{3.5}$ (25.8 mmol KOH g^{-1}), KP_2 (23.2 mmol KOH g^{-1}), and MCC_5 (19.4 mmol KOH g^{-1}). This suggests that an appropriate amount of lignin in the beads can support the porous structure to access the exposed hydroxyl groups (e.g., CRM_2) on both carbohydrates and lignin, which is consistent with the emergence of the micropores as observed by SEM (Fig. 2b). However, excess lignin may agglomerate to envelop the polysaccharides (Scheme 1c), thereby inhibiting the access of the hydroxyl groups on the pore walls (e.g., $POP_{3.5}$). For pure cellulosic beads, the higher –OH number of KP_2 than MCC_5 may mainly be explained by the presence of amorphous substance in KP_2 that has more accessible hydroxyl groups compared to MCC_5 that only the hydroxyl groups on the surface of microcrystalline are available.

The density of the beads was primarily related to the cellulose or lignocellulose load in the IL solution. Therefore, it is unsurprising that the MCC_5 and $POP_{3.5}$ beads had high densities (0.113 and 0.099 g cm^{-3}, respectively)and thus low porosities (93.2% and 94.2%, respectively; Table 1). The CRM_2 beads possessed the lowest density (0.042 g cm^{-3}) and thus the highest porosity (97.0%). At a comparable concentration level, the KP_2 exhibited higher density than the CRM_2, which can be attributed to formation of more hydrogen bonds, resulting in the collapse of the pores in the KP_2 beads. The water uptake ability of the beads seemed closely related to their porosity, with the water content of the CRM_2 beads being the highest (97.0%; Table 1).

Characterization of modified hydrogel beads

Functionalization efficacy during carboxymethylation

Carboxymethylation of the beads proceeded via etherification of the accessible hydroxyl groups of polysaccharides (mainly cellulose) with sodium monochloroacetate under alkaline condition (Scheme S1), resulting in formation of carboxymethylated beads, $CPOP_{3.5}$, $CCRM_2$, CKP_2 and $CMCC_5$. The degree of substitution (DS), the average number of substituent (here, carboxymethyl-) groups attached per base unit, was positively related to the number of accessible hydroxyl groups (Fig. 3a). Thus, the substitution efficacy of CRM_2 was almost three times higher than that of MCC_5, which further suggested the support effect of lignin in the CRM beads, allowing better access of monochloroacetate to the hydroxyl groups.

Functionalization efficacy during magnetization

To facilitate the removal of beads from solutions, we attempted the in situ synthesis of Fe_3O_4—one of the commonly-used magnetic adsorbents (Banerjee and Chen 2007; Mahdavi et al. 2012), into the structure of "original" beads with the precursor solution containing 15/30 mM $FeCl_2{\cdot}4H_2O/FeCl_3{\cdot}6H_2O$ via a hydrothermal method. The resultant magnetized beads, $MPOP_{3.5}$, $MCRM_2$, MKP_2 and $MMCC_5$, became black and the Fe_3O_4 content in the beads was determined by weighing the dry masses of the beads before and after magnetite incorporation. The results showed that the Fe_3O_4 content was reduced with increasing density of the original beads (Fig. 3b). The $MCRM_2$ beads had the highest Fe_3O_4 load, which is also consistent with their highest porosity and –OH number. $MPOP_{3.5}$ had a slightly higher Fe_3O_4 content than MKP_2 despite of the higher density, which can be attributed to the presence of the micropores in the $MPOP_{3.5}$.

Magnetized/carboxymethylated hydrogel beads

After dual functionalization, the magnetized/carboxymethylated beads were of brown color, different from the black color of the "magnetized only" beads (Fig. 4a, insets), which is consistent with the results reported in the literature (Nata et al. 2011; Tang et al. 2012). Under external magnetic field, magnetized/carboxymehylated beads exhibited a comparable saturation magnetization (M_s) value to that obtained for the "magnetized only" beads (Fig. 4a). This result revealed that the removal of Fe_3O_4 nanoparticles (Fig. S6) from the hydrogel beads during subsequent carboxymethylation was negligible, suggesting a strong interaction between the iron oxide and the lignocellulose polymers. The Fe_3O_4 aggregates were successfully precipitated on the bead's surface and lamellar walls as verified by SEM (Fig. 4b, c), exhibiting sizes ranging from tens to hundreds of nanometers.

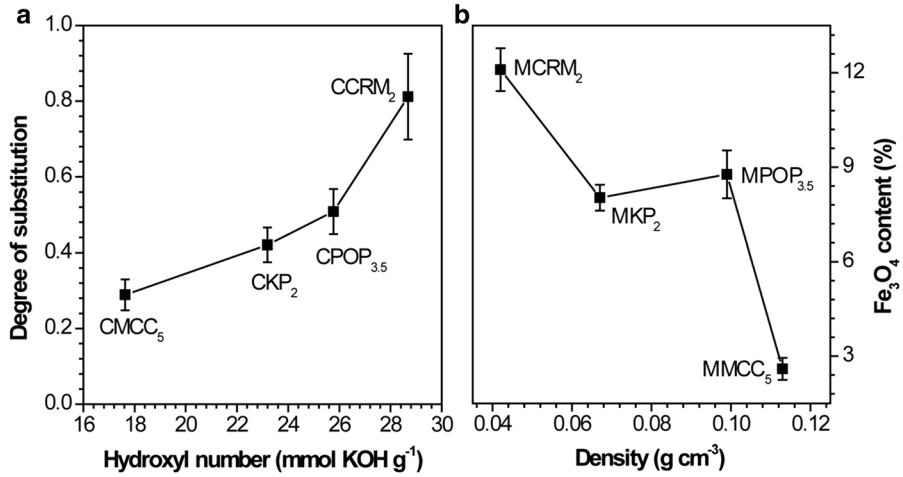

Fig. 3 **a** Effect of the hydroxyl number of the original beads on the degree of substitution (DS) of the carboxymethylated beads; and **b** effect of the density of the original beads on the content of Fe_3O_4 incorporated in the magnetized beads

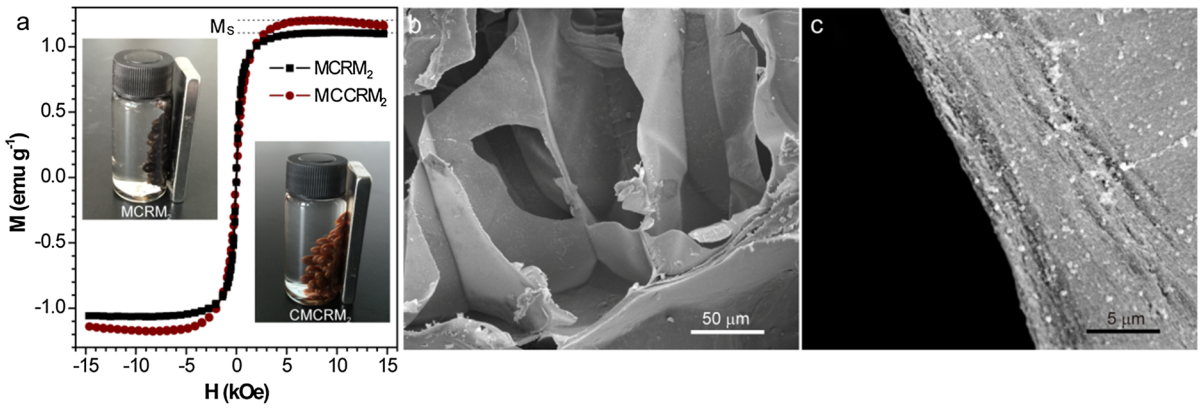

Fig. 4 **a** The field-dependent magnetization curves, and **b**, **c** the micrographs of the inner structure of the $MCCRM_2$ bead's lamellar walls at × 500 and × 5000 magnifications, respectively

Powder X-ray Diffraction (PXRD) of the magnetized beads exhibited (220), (311), (400), (422), and (511) planes at 2θ values of 30.0°, 35.3°, 43.0°, 53.5° and 57.0°, confirming the formation and introduction of black crystalline Fe_3O_4 in the beads (Fig. 5a) (Liu et al. 2016). The peaks' intensities of the magnetized/carboxymethylated beads hardly changed compared to those of the "magnetized only" beads, implying again the firm deposition of Fe_3O_4.

The success of etherification by sodium monochloroacetate was confirmed by the emergence of the 1595 cm^{-1} peak assigned to the carbonyl (C=O) asymmetric vibration of the carboxylate anions ($–COO^-$) in the FT-IR spectrum (Fig. 5b), in agreement with the literature value of 1605 cm^{-1} for carboxymethylated cellulose (Qi et al. 2009). Interestingly, after magnetization and carboxymethylation, the intensity of the carboxylate vibration peak in the functionalized beads ($MCCRM_2$) was considerably enhanced compared to the "carboxymethylated only" beads (Fig. 5b), suggesting that the number of carboxylate groups as adsorptive sites increased after

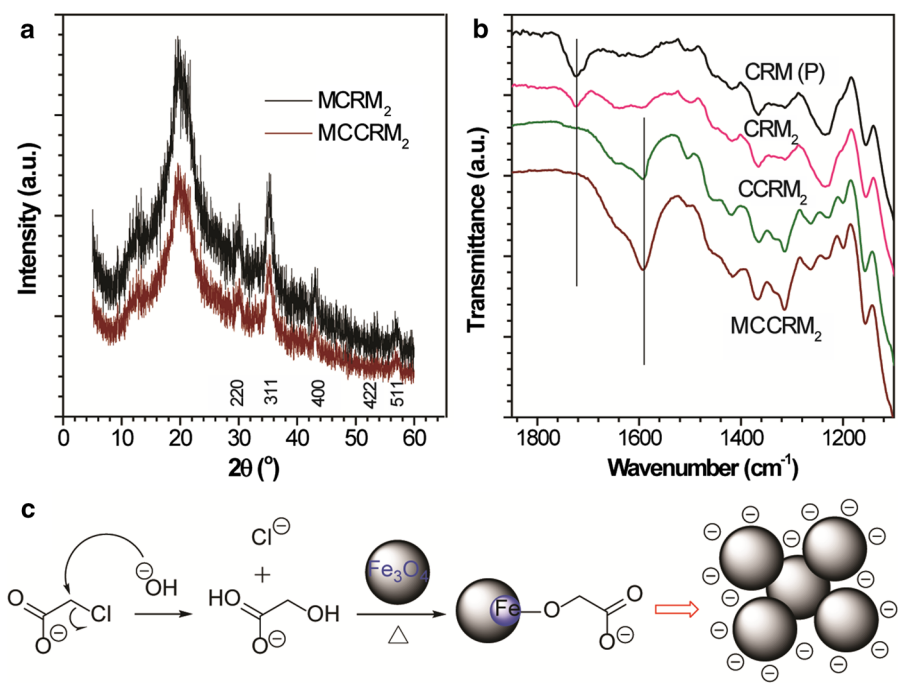

Fig. 5 **a** PXRD patterns and **b** FT-IR spectra of the functionalized beads ["(P)" represents "powder"]; and **c** the possible modes of covalent binding of monochloroacetate onto Fe_3O_4 incorporated in the beads according to Togashi et al. (2011)

combinative functionalization. This was most likely due to the occurrence of carboxymethylation not only on hydroxyl sites of carbohydrates, but also on the incorporated Fe_3O_4 nanoparticles in the beads via binding of hydrolyzed monochloroacetate to the atomic surface of Fe_3O_4 (Fig. 5c) (Togashi et al. 2011). Additionally, the hemicellulose peak at 1725 cm^{-1} (Sun et al. 2009) disappeared, suggesting the leaching out of hemicellulose after functionalization (Fig. 5b). This result indicates that functionalized lignocellulosic hydrogel beads consist mainly of lignin and cellulose.

Heavy metal adsorption

For evaluating the effects of lignin in the beads - "original" (O), "carboxymethylated" (C), "magnetized" (M), and "magnetized/carboxymethylated" (MC), on the adsorption ability, wet beads (0.01 g dry mass) were immersed in 25 mL of 0.1 mM $Cu(NO_3)_2{\cdot}3H_2O$ or $Pb(NO_3)_2$ solution with pH value varying from 4.0 to 6.0, followed by incubating at 25 °C for 24 h under shaking. After adsorption, the beads were removed and the absorbance of the ions in the solution was determined using an atomic absorption spectrophotometer (AAS).

The original hydrogel beads exhibited an ascending order of adsorption ability for Cu^{2+} and Pb^{2+}: MCC_5, KP_2, $POP_{3.5}$, and CRM_2 (Fig. 6), under the optimum conditions (pH 6 for Cu^{2+} and pH 5.3 for Pb^{2}; Fig. S7). This is consistent with the increased order in the number of hydroxyl groups (Table 1) on both carbohydrates and lignin that are the adsorptive site for the metal ions. Both lignocellulosic hydrogel beads ($POP_{3.5}$ and CRM_2) adsorbed more metal ions than the pure cellulosic beads (MCC_5 and KP_2), which can be explained by the presence of micropores on the pore walls (Fig. 2) and the greater porosity of the lignocellulosic beads (Table 1). $POP_{3.5}$ had higher lignin content but lower adsorption ability than CRM_2, suggesting again that an excessive amount of hydrophobic lignin likely agglomerates and resultantly encapsulates polysaccharide macromolecules and thus occludes the hydroxyl groups.

Carboxymethylation improved the adsorption for Cu^{2+} and Pb^{2+} compared to the original beads. For instance, $CCRM_2$ had adsorption for ions approximately 2.5 times the amount of the original CRM_2 due to the high degree of substitution, while the adsorption ability of $CMCC_5$ was around 1.6 times that of its original MCC_5 (Fig. 6). The improved adsorption capacity can be explained by the higher coordinating affinity of the carboxylate anions with the divalent metal ions than the hydroxyl groups (Kikuchi et al. 2006). Magnetization by in situ synthesizing Fe_3O_4 nanoparticles in the original beads also resulted in an increase in the adsorption for metal ions, especially for Cu^{2+}, most likely caused by the higher adsorption (mmol g^{-1}) of Fe_3O_4 for Cu^{2+} than for Pb^{2+} ions (Mahdavi et al. 2012).

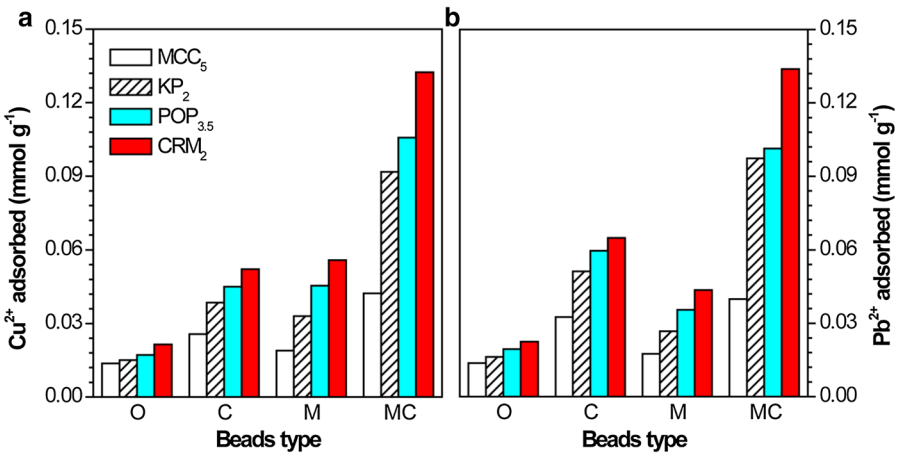

Fig. 6 The adsorption ability of the original (O), carboxymethylated (C), magnetic (M), and magnetized/carboxymethylated (MC) hydrogel beads for **a** Cu^{2+} and **b** Pb^{2+} ions [standard deviation < 0.004 mmol g^{-1}; 0.04 g dry weight of prepared gel beads in 100 mL of 0.1 mM $Cu(NO_3)_2{\cdot}3H_2O$ or $Pb(NO_3)_2$ solution; 24 h vibration, 25 °C, pH 6.0 for Cu^{2+} and 5.3 for Pb^{2+}]

The adsorptive capacity of the beads successively treated with magnetization and carboxymethylation exceeded the sum of the adsorption of the beads individually treated. For instance, $CCRM_2$ and $MCRM_2$ had more than double the capacity of the original CRM_2; after combinative treatment, the resultant magnetized/carboxymethylated beads loaded with carboxylate Fe_3O_4 exhibited an adsorption capacity around 0.13 mmol g^{-1} for both Cu^{2+} and Pb^{2+} ions (Fig. 6), which were 6 times of the adsorption of CRM_2. This may be explained by two reasons: (1) the number of carboxylate groups as adsorptive sites increased in the "MC" beads due to the carboxymethylation of both the hydroxyl groups on lignocellulose polymers and on Fe_3O_4 particles; and (2) Fe_3O_4 particles in the "MC" beads are covered with Fe–OH or $Fe–O^-$ groups in water, which can directly coordinate with Pb^{2+} and Cu^{2+} ions and form mono- and binuclear inner-sphere complexes (Horst et al. 2015; Mahdavi et al. 2012; Upadhyay et al. 2014). The adsorption was confirmed by the EDX spectra (Fig. S8).

Adsorption modeling analysis

The correlation between the adsorption capacity of the beads and the equilibrium concentration of the metal solution after adsorption was studied for $MCCRM_2$ which had the best adsorption ability among all the beads. It was found that the amount of metal adsorbed by the beads increased as the metal concentration in the solution increased, until the adsorption approached an equilibrium state (Fig. 7). The regression analyses of our experimental data for both Cu^{2+} and Pb^{2+} were shown to well correspond to the Langmuir relationship (R^2 = 0.985 and 0.996, Table 2), indicating homogeneous, monolayer adsorption. The calculated maximum adsorption capacity (q_m) reached 0.144 mmol g^{-1} and 0.161 mmol g^{-1} for Cu^{2+} and Pb^{2+}, respectively.

The Langmuir constant K_L derived from the Langmuir model is related to the affinity of the binding sites to the metal ions, that is, generally the higher adsorption, the larger K_L value. However, although the beads had a higher adsorption for Cu^{2+} ions than for Pb^{2+} at low concentrations (consistent with the higher K_L for Cu^{2+}), their adsorption at high concentrations or their q_m for Cu^{2+} was lower (Table 2). Volesky (2003) has reported this phenomenon, i.e., bio-adsorbents adsorbing better at low concentrations may be inferior at higher concentrations, and vice versa. In the case of high metal concentrations, the influence of the adsorbate nature including distribution coefficient (i.e., metal mobility in solution) and hydrated radius on the adsorption of the adsorbents may become larger. Pb^{2+} ions had a greater distribution coefficient (Li et al. 2011b) and a smaller hydrated radius (Qiu and Zheng 2009) than Cu^{2+} ions, hence justifying its growing uptake at high concentrations.

The Freundlich model assumes that the adsorbent has energetically heterogeneous surface and has different affinity for adsorption, in which the 1/n value is related to the degree of surface heterogeneity, i.e., smaller 1/n indicates more heterogeneous surface (Ngah and Fatinathan 2010). However, the low R^2 values illuminate again homogeneous adsorption of the beads towards metal ions. In the Sips isotherm

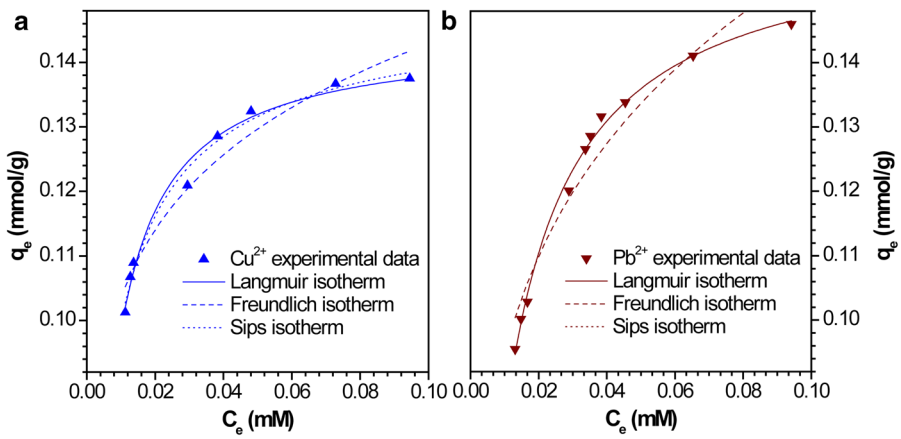

Fig. 7 Non-linear Langmuir, Freundlich and Sips isotherms for the adsorption of **a** Cu^{2+} and **b** Pb^{2+} ions onto the $MCCRM_2$ beads

Table 2 Constant parameters and correlation coefficients calculated using various isotherm models for the adsorption of Cu^{2+} and Pb^{2+} ions on $MCCRM_2$

Adsorption isotherms		Cu^{2+}	Pb^{2+}
Langmuir	q_m (mmol g^{-1})	0.144	0.161
	K_L (L $mmol^{-1}$)	215	110
	R^2	0.985	0.996
Freundlich	K_F (mmol g^{-1})	0.197	0.253
	1/n	0.140	0.213
	R^2	0.951	0.934
Sips	q_{max} (mmol g^{-1})	0.150	0.161
	K_S (L $mmol^{-1}$)	234	109
	β_S	0.793	1.002
	R^2	0.985	0.995

Table 3 Comparison of pseudo-first order, pseudo-second order and intraparticle diffusion kinetic models for the adsorption of Cu^{2+} and Pb^{2+} ions on $MCCRM_2$

Kinetic models		Cu^{2+}	Pb^{2+}
Pseudo-first order	k_1 (h^{-1})	0.192	0.164
	R^2	0.988	0.956
Pseudo-second order	k_2 (g $mmol^{-1}$ h^{-1})	5.89	5.81
	R^2	0.997	0.997
Intraparticle diffusion	$k_{int,1}$ (mmol g^{-1} $h^{1/2}$)	0.048	0.040
	$R^2_{int,1}$	0.998	0.990
	$k_{int,2}$ (mmol g^{-1} $h^{1/2}$)	0.023	0.024
	$C_{int,2}$ (mmol g^{-1})	0.037	0.021
	$R^2_{int,2}$	0.948	0.961
	$k_{int,3}$ (mmol g^{-1} $h^{1/2}$)	0.002	0.008
	$R^2_{int,3}$	0.761	0.941

model, since the β_S values are close to 1 (Table 2), the equations nearly reduce to the Langmuir equation.

From Fig. 8a, b and Table 3 it could be seen that the normalized standard deviation of pseudo-second order model was smaller than that of pseudo-first order model. Therefore, pseudo-second order model was more suitable to predict the ions adsorption process of beads in our experiments. As a result, it can be concluded that the chemical adsorption is dominant in the adsorption process, rather than physical adsorption described by the pseudo-first order model.

Intraparticle diffusion model was used to analyze the adsorption process, as shown in Fig. 8c. If the plot of q_t versus $t_{1/2}$ is multi-linear, other rate-limiting step along with intraparticle diffusion resistance also plays a major role on the adsorption process (Song et al. 2016). The overall rate of adsorption on the beads can be described by the following three steps (Ren et al. 2016): (1) surface diffusion of the sorbate from the bulk solution to the external surface of sorbent, which was controlled by the chemical adsorption, (2) intraparticle or pore diffusion of the sorbate molecules in the interior of sorbent, and (3) adsorption–desorption balance. Therefore, the overall rate of the adsorption process by the functionalized lignocellulosic beads was controlled by both surface diffusion and intraparticle diffusion.

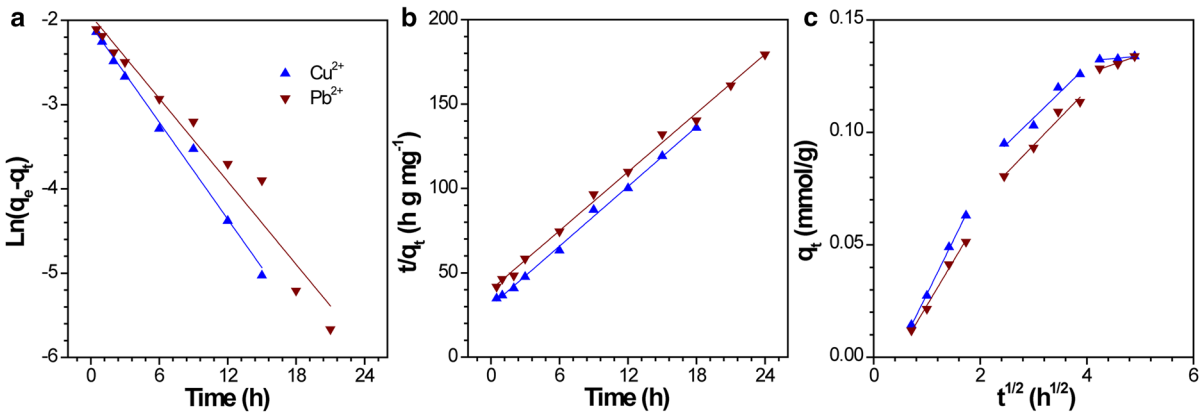

Fig. 8 **a** Pseudo-first order, **b** pseudo-second order and **c** intraparticle diffusion kinetics plots for the adsorption of Cu^{2+} and Pb^{2+} ions onto the $MCCRM_2$ beads

Conclusions

Lignocellulosic beads (CRM_2 and $POP_{3.5}$) exhibited the presence of micropores, and higher hydroxyl number and porosity compared to pure cellulosic beads (KP_2 and MCC_5) due to the porous structure support effect of the stiff lignin network, and thus higher functionalization efficacy after carboxymethylation and magnetization. Therefore, functionalized lignocellulosic beads had higher adsorption capacity for heavy metal ions than the analogous cellulosic beads, with maximum adsorption capacities (q_m) of 0.144 mmol g^{-1} and 0.161 mmol g^{-1} for Cu^{2+} and Pb^{2+}, respectively, derived from the Langmuir model. However, excessive lignin may agglomerate and occlude the adsorptive sites, thereby leading to a lower adsorption ability of the beads prepared directly from wood either before or after functionlization. Since lignocellulosic hydrogel beads can be obtained in a simpler, more economical and environmentally-friendly approach than pure cellulose beads, the preparation of lignocellulosic adsorbents may be more practical and competitive.

Acknowledgments Yanjun Xie thanks the financial support from the National Key Research and Development Program of China (2017YFD0600204).

References

Banerjee SS, Chen DH (2007) Fast removal of copper ions by gum arabic modified magnetic nano-adsorbent. J Hazard Mater 147:792–799

Barnett JR, Bonham VA (2004) Cellulose microfibril angle in the cell wall of wood fibres. Biol Rev 79:461–472

Chatterjee S, Lee MW, Woo SH (2010) Adsorption of congo red by chitosan hydrogel beads impregnated with carbon nanotubes. Bioresour Technol 101:1800–1806

Chen SY, Zou Y, Yan ZY, Shen W, Shi SK, Zhang X, Wang HP (2009) Carboxymethylated-bacterial cellulose for copper and lead ion removal. J Hazard Mater 161:1355–1359

Chen P, Yu HP, Liu YX, Chen WS, Wang XQ, Ouyang M (2013) Concentration effects on the isolation and dynamic rheological behavior of cellulose nanofibers via ultrasonic processing. Cellulose 20:149–157

Cheng FC, Wang H, Rogerst RD (2014) Oxygen enhances polyoxometalate-based catalytic dissolution and delignification of woody biomass in ionic liquids. ACS Sustain Chem Eng 2:2859–2865

Donia AM, Atia AA, Abouzayed FI (2012) Preparation and characterization of nano-magnetic cellulose with fast kinetic properties towards the adsorption of some metal ions. Chem Eng J 191:22–30

Driemeier C, Oliveira MM, Curvelo AAS (2016) Lignin contributions to the nanoscale porosity of raw and treated lignocelluloses as observed by calorimetric thermoporometry. Ind Crops Prod 82:114–117

Duchesne I, Hult E, Molin U, Daniel G, Iversen T, Lennholm H (2001) The influence of hemicellulose on fibril aggregation of kraft pulp fibres as revealed by FE-SEM and CP/MAS ^{13}C-NMR. Cellulose 8:103–111

Ferrer A, Quintana E, Filpponen I, Solala I, Vidal T, Rodriguez A, Rojas OJ (2012) Effect of residual lignin and heteropolysaccharides in nanofibrillar cellulose and nanopaper from wood fibers. Cellulose 19:2179–2193

Gan WT, Gao LK, Zhan XX, Li J (2016) Preparation of thiol-functionalized magnetic sawdust composites as an adsorbent to remove heavy metal ions. RSC Adv 6:37600–37609

Horst MF, Lassalle V, Ferreira ML (2015) Nanosized magnetite in low cost materials for remediation of water polluted with toxic metals, azo- and antraquinonic dyes. Front Environ Sci Eng 9:746–769

Jeon C, Kim JH (2009) Removal of lead ions using phosphorylated sawdust. J Ind Eng Chem 15:910–913

Kikuchi Y, Qian QR, Machida M, Tatsumoto H (2006) Effect of ZnO loading to activated carbon on Pb(II) adsorption from aqueous solution. Carbon 44:195–202

Kim CH, Youn HJ, Lee HL (2017) Preparation of surface-charged CNF aerogels and investigation of their ion adsorption properties. Cellulose 24:2895–2902

Labbe N, Rials TG, Kelley SS, Cheng ZM, Kim JY, Li Y (2005) FT-IR imaging and pyrolysis-molecular beam mass spectrometry: new tools to investigate wood tissues. Wood Sci Technol 39:61-U19

Li WY, Sun N, Stoner B, Jiang XY, Lu XM, Rogers RD (2011a) Rapid dissolution of lignocellulosic biomass in ionic liquids using temperatures above the glass transition of lignin. Green Chem 13:2038–2047

Li LJ, Liu FQ, Jing XS, Ling PP, Li AM (2011b) Displacement mechanism of binary competitive adsorption for aqueous divalent metal ions onto a novel IDA-chelating resin: isotherm and kinetic modeling. Water Res 45:1177–1188

Liu WJ, Jiang H, Yu HQ (2015) Thermochemical conversion of lignin to functional materials: a review and future directions. Green Chem 17:4888–4907

Liu S, Yao K, Fu LH, Ma MG (2016) Selective synthesis of Fe_3O_4, γ-Fe_2O_3, and α-Fe_2O_3 using cellulose-based composites as precursors. RSC Adv 6:2135–2140

Luo XG, Liu SL, Zhou JP, Zhang LN (2009) In situ synthesis of Fe_3O_4/cellulose microspheres with magnetic-induced protein delivery. J Mater Chem 19:3538–3545

Mahdavi S, Jalali M, Afkhami A (2012) Removal of heavy metals from aqueous solutions using Fe_3O_4, ZnO, and CuO nanoparticles. J Nanopart Res 14:171–188

Nata IF, Sureshkumar M, Lee CK (2011) One-pot preparation of amine-rich magnetite/bacterial cellulose nanocomposite and its application for arsenate removal. RSC Adv 1:625–631

Ngah WSW, Fatinathan S (2008) Adsorption of Cu(II) ions in aqueous solution using chitosan beads, chitosan-GLA beads and chitosan-alginate beads. Chem Eng J 143:62–72

Ngah WSW, Fatinathan S (2010) Adsorption characterization of Pb(II) and Cu(II) ions onto chitosan-tripolyphosphate

beads: kinetic, equilibrium and thermodynamic studies. J Environ Manag 91:958–969

Pokhrel D, Viraraghavan T (2004) Treatment of pulp and paper mill wastewater—a review. Sci Total Environ 333:37–58

Qi HS, Liebert T, Meister F, Heinze T (2009) Homogenous carboxymethylation of cellulose in the NaOH/urea aqueous solution. React Funct Polym 69:779–784

Qiu W, Zheng Y (2009) Removal of lead, copper, nickel, cobalt, and zinc from water by a cancrinite-type zeolite synthesized from fly ash. Chem Eng J 145:483–488

Ren H, Gao Z, Daoji W, Jiang J, Sun Y, Luo C (2016) Efficient Pb(II) removal using sodium alginate–carboxymethyl cellulose gel beads: preparation, characterization, and adsorption mechanism. Carbohydr Polym 137:402–409

Sciban M, Klasnja M, Skrbic B (2006) Modified softwood sawdust as adsorbent of heavy metal ions from water. J Hazard Mater 136:266–271

Sehaqui H, de Larraya UP, Liu P, Pfenninger N, Mathew AP, Zimmermann T, Tingaut P (2014) Enhancing adsorption of heavy metal ions onto biobased nanofibers from waste pulp residues for application in wastewater treatment. Cellulose 21:2831–2844

Shen X, Shamshina JL, Berton P, Gurau G, Rogers RD (2016a) Hydrogels based on cellulose and chitin: fabrication, properties, and applications. Green Chem 18:53–75

Shen X, Shamshina JL, Berton P, Bandomir J, Wang H, Gurau G, Rogers RD (2016b) Comparison of hydrogels prepared with ionic liquid-isolated vs. commercial chitin and cellulose. ACS Sustain Chem Eng 4:471–480

Song G, Zhu X, Chen R, Liao Q, Ding YD, Chen L (2016) An investigation of CO_2 adsorption kinetics on porous magnesium oxide. Chem Eng J 283:175–183

Sun N, Rahman M, Qin Y, Maxim ML, Rodriguez H, Rogers RD (2009) Complete dissolution and partial delignification of wood in the ionic liquid 1-ethyl-3-methylimidazolium acetate. Green Chem 11:646–655

Sun N, Jiang XY, Maxim ML, Metlen A, Rogers RD (2011) Use of polyoxometalate catalysts in ionic liquids to enhance the dissolution and delignification of woody biomass. Chemsuschem 4:65–73

Tang YL, Liang S, Yu SL, Gao NY, Zhang J, Guo HC, Wang YL (2012) Enhanced adsorption of humic acid on amine functionalized magnetic mesoporous composite microspheres. Colloids Surf A 406:61–67

Tang H, Zhou WJ, Lu A, Zhang LN (2014) Characterization of new sorbent constructed from Fe_3O_4/chitin magnetic beads for the dynamic adsorption of Cd^{2+} ions. J Mater Sci 49:123–133

Thakur S, Govender PP, Mamo MA, Tamulevicius S, Mishra YK, Thakur VK (2017) Progress in lignin hydrogels and nanocomposites for water purification: future perspectives. Vacuum 146:342–355

Thakur S, Sharma B, Verma A, Chaudhary J, Tamulevicius S, Thakur VK (2018) Recent progress in sodium alginate based sustainable hydrogels for environmental applications. J Clean Prod 198:143–159

Thakura VK, Thakur MK (2015) Recent advances in green hydrogels from lignin: a review. Int J Biol Macromol 72:834–847

Togashi T, Naka T, Asahina S, Sato K, Takami S, Adschiri T (2011) Surfactant-assisted one-pot synthesis of superparamagnetic magnetite nanoparticle clusters with tunable cluster size and magnetic field sensitivity. Dalton Trans 40:1073–1078

Upadhyay RK, Soin N, Roy SS (2014) Role of graphene/metal oxide composites as photocatalysts, adsorbents and disinfectants in water treatment: a review. RSC Adv 4:3823–3851

Volesky B (2003) Sorption and biosorption. Equilibrium biosorption performance. BV Sorbex, St. Lambert, Québec, pp 103–116

Wang H, Gurau G, Rogers RD (2012) Ionic liquid processing of cellulose. Chem Soc Rev 41:1519–1537

Wu ZM, Cheng ZH, Ma W (2012) Adsorption of Pb(II) from glucose solution on thiol-functionalized cellulosic biomass. Bioresour Technol 104:807–809

Yu XL, Tong SR, Ge MF, Wu LY, Zuo JC, Cao CY, Song WG (2013) Adsorption of heavy metal ions from aqueous solution by carboxylated cellulose nanocrystals. J Environ Sci 25:933–943